



Three years of *Galileo* dust data

E. Grün,¹ M. Baguhl,¹ N. Divine,² H. Fechtig,¹ D. P. Hamilton,¹ M. S. Hanner,² J. Kissel,¹ B.-A. Lindblad,³ D. Linkert,¹ G. Linkert,¹ I. Mann,⁴ J. A. M. McDonnell,⁵ G. E. Morfill,⁶ C. Polansky,² R. Riemann,¹ G. Schwehm,⁷ N. Siddique,¹ P. Staubach¹ and H. A. Zook⁸

¹Max-Planck-Institut für Kernphysik, 69029 Heidelberg, Germany

²Jet Propulsion Laboratory, Pasadena, CA 91109, U.S.A.

³Lund Observatory, 221 Lund, Sweden

⁴Max-Planck-Institut für Aeronomie, 37191 Katlenburg-Lindau, Germany

⁵University of Kent, Canterbury CT2 7NR, U.K.

⁶Max-Planck-Institut für Extraterrestrische Physik, 85748 Garching, Germany

⁷ESTEC, 2200 AG Noordwijk, The Netherlands

⁸NASA Johnson Space Center, Houston, TX 77058, U.S.A.

Received 14 September 1994; revised 7 November 1994; accepted 9 December 1994

Abstract. From its launch in October 1989 until the end of 1992, the *Galileo* spacecraft traversed interplanetary space from Venus to the asteroid belt and successfully executed close flybys of Venus, the Earth, and the asteroid Gaspra. The dust instrument has been operating most of the time since it was switched on in December 1989. Except for short time intervals near Earth, data from the instrument were received via occasional (once per week to once per month) memory read outs containing 282–818 bytes of data. All events (impacts or noise events) were classified by an onboard program into 24 categories. Over the three-year time span, the dust detector recorded 469 “big” dust impacts. These were counted in 21 of the 24 event categories. The three remaining categories of very low amplitude events contain mostly noise events. The impact rate varied from 0.2 to 2 impacts per day depending on heliocentric distance and direction of spacecraft motion with respect to the interplanetary dust cloud. Because the average data transmission rate was very low, some data were not received on the ground. Complete data sets for 358 “big” impacts were received, but the other 111 “big” impacts were only counted. The observed impact rates are compared with a model of the meteoroid complex.

Introduction

The *Galileo* Dust Detector System (DDS) and the twin sensor on board *Ulysses* are highly sensitive multi-coinci-

Correspondence to: E. Grün

dence impact ionization detectors which have been described in detail by Grün *et al.* (1992c, d). In addition, data from the *Galileo* dust experiment have been published at various stages of the mission. Initial measurements and instrument performance are presented by Grün *et al.* (1992a, b) and Baguhl *et al.* (1992). Grün *et al.* (1994) discuss the possibility that some dust impacts may have originated from comet Shoemaker–Levy 9. Detection of interstellar dust by the *Galileo* dust instrument is described by Baguhl *et al.* (1994). Dust measurements during flybys of comets and asteroids are considered by Riemann and Grün (1992) and Hamilton and Burns (1992). Divine (1993) used the first year and a half of *Galileo* data as input to his interplanetary meteoroid model.

This is the second paper in a three paper set dedicated to presenting both raw and reduced dust impact data for analysis by researchers external to the *Galileo* and *Ulysses* Dust Teams. Paper I (Grün *et al.*, 1995b) gives details on the reduction process of *Galileo* and *Ulysses* dust data and Paper III (Grün *et al.*, 1995a) contains the first two years of *Ulysses* dust data. The current paper presents *Galileo* dust impact data from December 1989 to the end of 1992. The main data products are a table of the impact rates of all “big” impacts and a table of both raw and reduced data of all “big” impacts received on the ground. The information presented in these three papers is equivalent to data which we are submitting to the various data archiving centers (Planetary Data System, NSSDC, etc.).

Mission and instrument operations

During its initial phase the *Galileo* mission explored the solar system between Venus (0.7 AU) and the asteroid

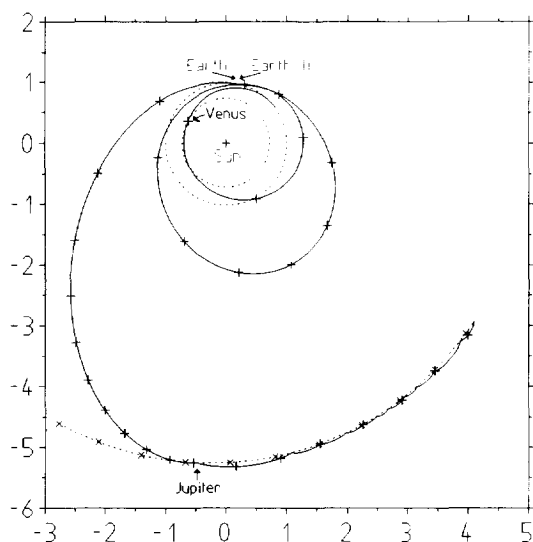


Fig. 1. Interplanetary trajectory of the *Galileo* spacecraft (solid) shown with the orbits of Venus, Earth and Jupiter (dashed). Planetary flybys are indicated and the tick marks correspond to 100 days of orbital motion

belt (2.3 AU); its orbit is shown in Fig. 1. Orbital elements, which match the actual *Galileo* interplanetary trajectory to an accuracy of 700,000 km, are provided in Table 1. After launch on October 18, 1989, *Galileo* flew to Venus which it passed on February 10, 1990. On December 8, 1990 *Galileo* swung by the Earth which sent it onto an orbit with an aphelion in the asteroid belt. After returning to Earth two years later, *Galileo* obtained enough energy to reach Jupiter in December 1995. The *Galileo* mission and spacecraft are described by Johnson *et al.* (1992) and D'Amario *et al.* (1992). The *Galileo* spacecraft is a dual-spinning spacecraft with its antenna pointed antiparallel to the spin vector. During most of the mission, the antenna pointed approximately towards the Sun; deviations from the Sun pointing are shown in Fig. 2. In 1991 and 1992, the spacecraft was repeatedly turned away from the Sun in efforts to cool, and thereby free, the spacecraft high gain antenna which failed to deploy in April 1991. Unfortunately, these attempts were unsuccessful.

The dust detector is mounted on the spinning section of the spacecraft and the sensor axis is offset by an angle of 55° with respect to the positive spin axis (opposite to the antenna direction). Because of the spacecraft spin and the 140° opening angle of the sensor, the dust detector is always able to sense particles that are within 15° of the positive spin axis. Over a complete rotation cycle, all angles within 125° of the spin axis are sampled. The rotation angle is defined as follows. First, project the dust detector axis onto a plane perpendicular to the spacecraft spin axis. The rotation angle (ROT) is measured in this plane with 0° defined as closest to ecliptic north. For both *Ulysses* and *Galileo*, 90° is close to the direction in which particles on prograde uninclined circular orbits move; with this pointing, the dust detectors are most sensitive to particles on retrograde orbits. During the initial portion of the mission there were rather long time periods when no sector (rotation angle) information was provided by the spacecraft to the instruments. Therefore, during these

Table 1. Orbital elements of the *Galileo* trajectory from launch until the end of 1992 (1 AU = 149, 597, 871 km)

Orbital elements	Valid time range (error < 700,000 km)	
<i>Earth to Venus</i>		
Epoch	1989 Nov. 9 16:30:56	
Perihelion	0.66769 AU	
Eccentricity	0.19775	1989–360 00:00
Inclination	4.3260	to
Long. of asc. node	24.70	1990–041 00:00
Arg. of perihelion	184.80	
Mean anomaly	201.57	
True anomaly	194.82	
<i>Venus to Earth I</i>		
Epoch	1990 Apr. 30 00:00:00	
Perihelion	0.69785 AU	
Eccentricity	0.29445	1990–041 00:00
Inclination	3.3818	to
Long. of asc. node	75.89	1990–342 00:00
Arg. of perihelion	106.70	
Mean anomaly	63.862	
True anomaly	97.819	
<i>Earth I to Earth II</i>		
Epoch	1991 Sep. 10 12:00:00	
Perihelion	0.90427 AU	
Eccentricity	0.43029	1990–342 00:00
Inclination	4.5473	to
Long. of asc. node	255.87	1992–344 00:00
Arg. of perihelion	223.14	
Mean anomaly	119.42	
True anomaly	151.68	
<i>Post Earth II orbit</i>		
Epoch	1992 Dec. 11 20:08:20	
Perihelion	0.98246 AU	
Eccentricity	0.68756	1992–344 00:00
Inclination	1.5228	to
Long. of asc. node	255.91	1992–365 00:00
Arg. of perihelion	186.49	
Mean anomaly	359.73	
True anomaly	358.01	

periods the direction of dust impacts could not be determined.

The *Galileo* spacecraft returns dust impact data in two ways. When the spacecraft is close enough to the Earth to support high data rates, data from the dust experiment are received nearly continuously at a rate of 24 bits per second as part of the Low Rate Science (LRS) telemetry. This LRS data were available during a four-day initial check-out period in December 1989 and during 2 two-month periods around both Earth flybys in December 1990 and December 1992. During the remainder of the time, data from the dust instrument were transmitted as instrument memory read-outs (MROs). The MROs returned event data which had accumulated over time in the instrument memory. The MROs were obtained during intervals of contact with the Deep Space Network (DNS), occurrences of which varied from once every few days to once per month. Initially, a MRO contained 14 instrument data frames (with each frame comprising the complete data set of an impact or noise event, consisting of 128 bits, plus ancillary and engineering data). In June 1990, the

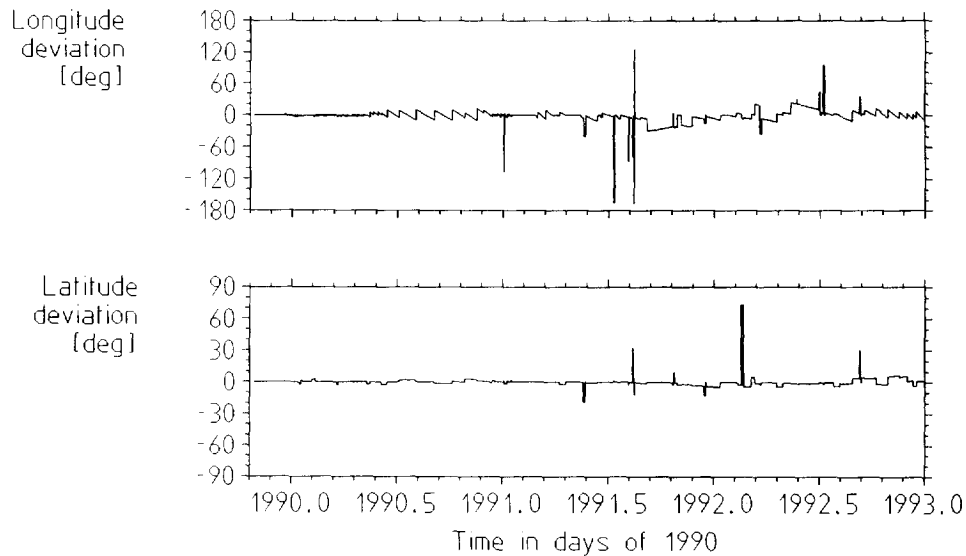


Fig. 2. Spacecraft attitude: deviation of the high gain antenna pointing (i.e. negative spin axis) from the Sun direction. The angles are given in a coordinate system referenced to the mean ecliptic and equinox of 1950.0

onboard program was changed to increase the size of a MRO from 14 to 40 instrument data frames.

Significant mission and dust instrument events are listed in Table 2. The dust instrument was switched on three weeks after launch, after which dust measurements and noise tests commenced. In initial noise tests, the dust instrument was set to its highest sensitivity state and the noise environment was characterized. During most of the remaining time, the instrument was kept in a state where approximately 10 clearly identifiable noise events occurred per day. During flybys of the Earth and Venus, however, noise rates were strongly enhanced (Baguhl *et al.*, 1992). Several anomalies on board the *Galileo* spacecraft caused the dust instrument to be unable to collect data for a total of 176 days.

The nominal channeltron high voltage (HV step 4 = 1250 V) could not be set because of unexpected noise which was also problematic for the *Ulysses* detector. It is assumed that the nearby radioactive thermal generators (RTGs) are responsible for this noise, although other reasons cannot be excluded. During ground tests (without RTGs) no such noise was observed.

Temporary noise sources with external causes include energetic particles from solar flares and from planetary radiation belts (Baguhl *et al.*, 1992, 1994). Figures 3a and b show the noise rate during each of the Earth flybys. High count rates (about 1 noise event per second) were encountered for about 30 min during the 1990 crossing of the radiation belts. As a consequence, during the second Earth encounter the sensitivity of the measurement channels was reduced by two steps for the 2 h around closest approach. Enhanced noise rates were recorded for more than 10 h around the 1992 closest approach and, despite the reduction in the sensitivity, significant noise was still recorded in the hour around closest approach. Examination of the data revealed that during both crossings of the Earth's radiation belts, noise events were recorded in low-amplitude event categories which normally contain only dust impacts.

With *Ulysses*, the time of an impact or noise event is recorded with a 2 s accuracy. *Galileo*, however, cannot always return such accurate timings because of its crippled antenna. During periods of low rate science transmission, the instrument time resolution was set to “short time” which is defined as 0.67 s. During periods of MRO transmission, however, the time resolution was changed to “long time” which was initially set to 1.1 h but redefined by the reprogramming in June 1990 to 4.3 h. The “long-time” mode is necessary when the interval between subsequent MROs is long (>170 s; the memory location where the time is stored is an 8 bit word allowing the identification of only 256 unique times). The definition of long time was changed to the larger value in order to determine uniquely the time interval during which each impact occurred even if subsequent MROs are a month apart.

Impact events

All events, dust impacts and noise, are classified into one of 24 different categories (6 amplitude ranges and 4 event classes) and counted in 24 corresponding accumulators (Paper I). Most of the accumulators are relatively free from noise; except for extreme situations, such as radiation belt crossings, they count only real impacts. Only the low amplitude and class categories—AC01 (event class 0, amplitude range 1), AC11, and AC02—are strongly contaminated by noise. We call the dust particles detected in the noise-free accumulators “big” impacts. The search for an analysis of true “small” impacts in the noisy categories of *Galileo* events (cf. Baguhl *et al.* (1993) for *Ulysses* data) is forthcoming. The situation is more complicated than for *Ulysses* because many of the measurements in the noisy categories could not be transmitted to Earth before they were overwritten.

Table 3 displays the number of “big” dust impacts

Table 2. *Galileo* mission and dust detector (DDS) configurations, tests, and other events

Yr-DOY	Date	Time	Event
89-291	(18 Oct. 1989)		<i>Galileo</i> launch
89-361	(27 Dec. 1989)	19:18	DDS cover release
89-362	(28 Dec. 1989)	17:20	<i>Galileo</i> LRS start
89-362	(28 Dec. 1989)	17:20	DDS on, noise test and configuration: HV = 4, EVD = C, I, E, SSEN = 0, 0, 0, 0, short time
89-363	(29 Dec. 1989)	01:02	DDS noise test and configuration: HV = 2
89-363	(29 Dec. 1989)	19:32	DDS configuration: EVD = C, I
89-364	(30 Dec. 1989)	17:45	DDS configuration: EVD = I, E, SSEN = 0, 0, 1, 0, long time
89-365	(31 Dec. 1989)	00:05	DDS configuration: EVD = I
89-365	(31 Dec. 1989)	00:30	<i>Galileo</i> LRS end
90-009	(9 Jan. 1990)	00:20	DDS first MRO after LRS
90-041	(10 Feb. 1990)	05:59	<i>Galileo</i> Venus flyby
90-047	(16 Feb. 1990)	22:11	DDS configuration: SSEN = 1, 0, 1, 0
90-176	(25 June 1990)	14:45	DDS reprogramming
90-306	(5 Nov. 1990)	17:00	<i>Galileo</i> LRS start
90-312	(8 Nov. 1990)	17:30	DDS noise test and configuration: SSEN = 1, 0, 1, 1, short time
90-316	(12 Nov. 1990)	17:30	DDS noise test and configuration: EVD = I
90-318	(14 Nov. 1990)	17:30	DDS noise test
90-319	(15 Nov. 1990)	19:30	DDS noise test
90-342	(8 Dec. 1990)	20:34	<i>Galileo</i> first Earth flyby
90-346	(11 Dec. 1990)	17:30	DDS noise test
90-347	(12 Dec. 1990)	22:05	DDS configuration: EVD = C, I, SSEN = 0, 0, 1, 1
90-349	(14 Dec. 1990)	22:00	DDS configuration: long time
90-365	(31 Dec. 1990)	18:00	<i>Galileo</i> LRS end
91-121	(1 May 1991)	16:35	DDS last MRO before anomaly
91-123	(3 May 1991)	05:26	<i>Galileo</i> in safe mode and DDS memory corrupted
91-190	(9 July 1991)	19:50	DDS off
91-198	(17 July 1991)	17:00	DDS on and configuration: HV = 2, EVD = C, I, SSEN = 0, 0, 1, 1, long time
91-201	(20 July 1991)	02:09	<i>Galileo</i> in safe mode and DDS memory corrupted
91-217	(13 Aug. 1991)	09:45	DDS off
91-228	(16 Aug. 1991)	01:20	DDS on and configuration: HV = 2, EVD = C, I, SSEN = 0, 0, 1, 1, long time
91-302	(30 Oct. 1991)	22:37	<i>Galileo</i> Gaspia flyby
91-337	(3 Dec. 1991)	21:01	DDS last MRO before switch-off
91-340	(6 Dec. 1991)	22:30	DDS off, <i>Galileo</i> cold turn
91-350	(16 Dec. 1991)	22:00	DDS on and configuration: HV = 2, EVD = C, I, SSEN = 0, 0, 1, 1, long time
92-023	(23 Jan. 1992)	19:45	DDS last MRO before switch-off
92-028	(28 Jan. 1992)	22:30	DDS off, <i>Galileo</i> cold turn
92-065	(5 Mar. 1992)	07:50	DDS on and configuration: HV = 2, EVD = C, I, SSEN = 0, 0, 1, 1, long time
92-092	(2 Apr. 1992)	18:49	DDS last MRO before switch-off
92-097	(6 Apr. 1992)	23:00	DDS off, <i>Galileo</i> cold turn
92-107	(16 Apr. 1992)	18:05	DDS on and configuration: HV = 2, EVD = C, I, SSEN = 0, 0, 1, 1, long time
92-308	(3 Nov. 1992)	00:48	<i>Galileo</i> LRS start
92-310	(5 Nov. 1992)	07:04	DDS configuration: short time
92-328	(23 Nov. 1992)	17:00	DDS noise test
92-336	(1 Dec. 1992)	16:30	DDS noise test
92-338	(3 Dec. 1992)	16:00	DDS noise test
92-339	(4 Dec. 1992)	16:30	DDS noise test
92-343	(8 Dec. 1992)	14:09	DDS configuration, HV = 1, EVD = I, SSEN = 2, 0, 2, 2
92-343	(8 Dec. 1992)	15:09	<i>Galileo</i> second Earth flyby
92-343	(8 Dec. 1992)	16:09	DDS configuration, HV = 2, EVD = C, I, SSEN = 0, 0, 1, 1
92-349	(14 Dec. 1992)	11:00	DDS configuration: long time
92-354	(19 Dec. 1992)	02:39	<i>Galileo</i> LRS end

Abbreviations used to describe the instrument configuration: LRS, data transmission in Low Rate Science format; MRO, DDS memory read-out; HV, channeltron high voltage step; EVD, event definition, ion- (I), channeltron- (C), or electron-channel (E); SSEN, detection thresholds ICP, CCP, ECP, and PCP; short time, time resolution 2/3 s; long time, time resolution 1 h before 90-176, 4 h after 90-176.

recorded in intervals of seven days or longer, depending on the occurrence of MROs. When the frequency of MROs was higher or when no impact was recorded, MROs are lumped together. The instrument was shut down five times, sometimes intentionally to protect it from direct solar radiation during Sun-pointing periods and at

other times when the data were corrupted unintentionally by spacecraft anomalies. These breaks are indicated as solid lines in Table 3. The largest gap appears between days 91–121 and 91–228: the instrument was switched off and on twice, but no useful data were recorded over the entire three and a half months. During the initial three

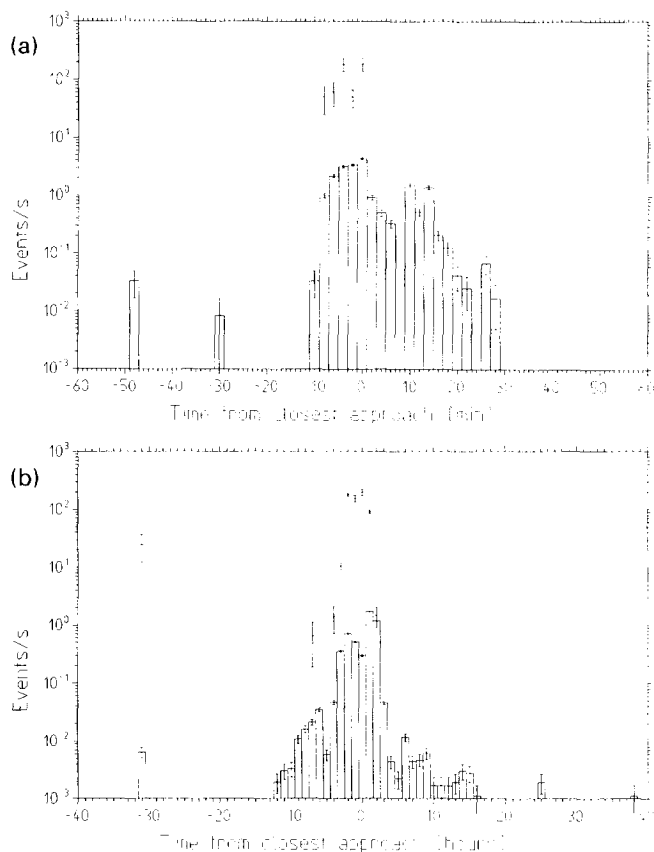


Fig. 3. Noise count rates during Earth flybys. Event counters (bars) saturate at about 20 events per second while the special noise counters saturate at about 200 events. (a) *Galileo* had its first close approach with the Earth on December 8, 1990 at 20.34 hours UT. Instrument threshold (ICP) was set to step one. The event counts were averaged over 2 min. (b) The second Earth flyby occurred on December 8, 1992, 15.09 hours. For 2 h around closest approach, the sensitivity threshold (ICP) was increased from step 0 to step 2

years of the *Galileo* mission, the instrument detected 469 “big” dust impacts. Since both the dust impact and noise rates were low during most of this period it is expected that, when the instrument was on, no “big” dust impacts were missed.

Radiation belts provide a noisy environment for the instrument. During the two Earth flybys, 528 clearly identified noise events were logged in normally noise-free categories. Here we give the accumulator name followed by the numbers of noise events detected during the 1990 and 1992 Earth encounters: AC21 (191/139), AC12 (74/66), AC22 (39/2), AC03 (0/10), AC13 (0/4), and AC23 (0/1). These events are not included in Table 3. The noise rate as a function of time during the two Earth flybys is given in Figs 3a and b. During several hours around Earth closest approaches, and in a much reduced manner during the Venus flyby, the increased noise rate caused significant dead-time.

Figure 4 shows the impact rate of dust particles recorded by the *Galileo* dust detector up until the end of 1992. At the same heliocentric distance, the impact rates were lower by about a factor ten when the spacecraft moved towards the Sun compared to the rates measured when it moved away from the Sun. This effect is due to

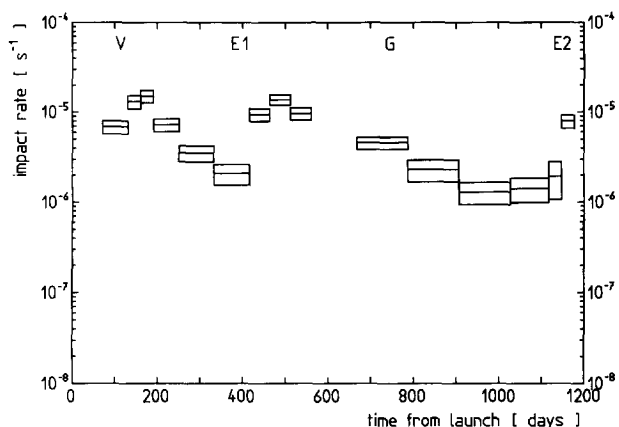


Fig. 4. Impact rates as a function of time are shown for “big” impacts. The thick bars give the average fluxes in the indicated intervals. The boxes indicate the 1-sigma error. Flybys of Venus (V), Earth (E1 and E2) and Gaspra (G) are indicated

the fact that the dust detector looks away from the Sun; when *Galileo* has a positive radial velocity, the instrument’s field of view includes the ram direction. After both Earth flybys, the impact rate increased by about an order of magnitude for a similar reason. Each flyby increased *Galileo*’s radial velocity, thereby making the instrument more sensitive to dust on low eccentricity orbits. Finally, during the Gaspra flyby no enhancement above the average impact rate (0.3 per day) was observed in agreement with the prediction of Hamilton and Burns (1992).

With the help of the elaborate memory storage concept of the dust instrument, complete data for 358 impacts were received on the ground. In the original memory setup, only “class 3” events were stored in a safe portion of the memory that would not be overwritten by lower-class events. Because of the long time between subsequent MROs, however, about 50% of the data for impacts in other classes were being overwritten before they could be transmitted to ground. The problem was remedied in June 1990 when the instrument was reprogrammed with a new data storage and transmission scheme. The improvement allows us to store and subsequently transmit several events of all categories in a single MRO. In addition, the content of a MRO was increased by about a factor 3—with this scheme complete data of 95% of all recorded “big” impacts were received on the ground after June 1990.

A list of the 358 “big” impacts for which complete information exists is displayed in Table 4. Dust particles are identified by their sequence number and their impact time. The event category—class (CLN) and amplitude range (AR)—is also given. Raw data as received on ground are displayed next: sector value (SEC) at time of impact, impact charge numbers (IA, EA, CA) and rise times (IT, ET), time difference and coincidence of electron and ion signals (EIT, EIC), coincidence of ion and channeltron signal (IIC), and charge reading at the entrance grid (PA) as well as time (PET) between this signal and the impact. This is followed by instrument status information such as event definition (EVD), charge sensing thresholds (ICP, ECP, CCP, PCP) and channeltron high voltage step (HV, see Paper I for further explanations).

Orbital information follows next: heliocentric distance

Table 3. (*Continued*)

Date	Time	r(AU)	Δt (d)	AC 01	AC 11	AC 21	AC 31	AC 02	AC 12	AC 22	AC 32	AC 03	AC 13	AC 23	AC 33	AC 04	AC 14	AC 24	AC 34	AC 05	AC 15	AC 25	AC 35	AC 06	AC 16	AC 26	AC 36
91-007	18:43	0.906	7.1	*	*	-	-	*	2	-	1	-	-	-	-	-	-	-	-	-	-	-	-	-	-	-	-
91-014	18:09	0.906	7.0	*	*	-	-	*	-	-	-	-	-	-	-	-	-	-	-	-	-	-	-	-	-	-	-
91-021	19:09	0.913	7.0	*	*	-	2	*	1	-	1	-	-	-	-	-	-	-	-	-	-	-	-	-	-	-	-
91-028	17:25	0.928	6.9	*	*	-	2	*	1	-	1	-	-	-	-	-	-	-	-	-	-	-	-	-	-	-	-
91-035	17:24	0.949	7.0	*	*	-	1	*	-	-	2	-	-	-	-	-	-	-	-	-	-	-	-	-	-	-	-
91-044	17:19	0.985	9.0	*	*	-	2	*	1	-	1	-	-	-	-	-	-	-	-	-	-	-	-	-	-	-	-
91-053	16:44	1.029	9.0	*	*	-	-	*	6	-	1	-	-	-	-	-	-	-	-	-	-	-	-	-	-	-	-
91-065	18:29	1.096	12.1	*	*	-	1	*	4	-	1	-	-	-	-	-	-	-	-	-	-	-	-	-	-	-	-
91-074	18:09	1.151	9.0	*	*	-	1	*	2	-	1	-	-	-	-	-	-	-	-	-	-	-	-	-	-	-	-
91-084	18:40	1.215	10.0	*	*	-	3	*	2	-	2	-	-	-	-	-	-	-	-	-	-	-	-	-	-	-	-
91-121	16:39	1.453	36.9	*	*	-	3	*	5	-	1	-	-	-	-	-	-	-	-	-	-	-	-	-	-	-	-
91-228	01:20	1.995	106.4	*	*	-	-	*	-	-	-	-	-	-	-	-	-	-	-	-	-	-	-	-	-	-	-
91-253	14:14	2.082	25.5	*	*	-	2	*	2	-	2	-	-	-	-	-	-	-	-	-	-	-	-	-	-	-	-
91-280	15:03	2.156	27.0	*	*	-	2	*	1	-	2	-	-	-	-	-	-	-	-	-	-	-	-	-	-	-	-
91-296	21:37	2.192	16.3	*	*	-	-	*	1	-	2	-	-	-	-	-	-	-	-	-	-	-	-	-	-	-	-
91-303	04:57	2.204	6.3	*	*	-	-	*	1	-	1	-	-	-	-	-	-	-	-	-	-	-	-	-	-	-	-
91-315	00:02	2.225	12.8	*	*	-	-	*	1	-	2	-	-	-	-	-	-	-	-	-	-	-	-	-	-	-	-
91-328	20:32	2.242	12.9	*	*	-	1	*	1	-	2	-	-	-	-	-	-	-	-	-	-	-	-	-	-	-	-
91-337	21:02	2.252	9.0	*	*	-	-	*	-	-	3	-	-	-	-	-	-	-	-	-	-	-	-	-	-	-	-
91-350	20:00	2.262	13.0	*	*	-	-	*	-	-	-	-	-	-	-	-	-	-	-	-	-	-	-	-	-	-	-
91-364	21:11	2.269	14.0	*	*	-	-	*	1	-	1	-	-	-	-	-	-	-	-	-	-	-	-	-	-	-	-
92-013	19:31	2.270	13.9	*	*	-	1	*	-	-	-	-	-	-	-	-	-	-	-	-	-	-	-	-	-	-	-
92-065	07:50	2.234	51.5	*	*	-	-	*	-	-	-	-	-	-	-	-	-	-	-	-	-	-	-	-	-	-	-
92-073	16:32	2.222	8.4	*	*	-	1	*	1	-	1	-	-	-	-	-	-	-	-	-	-	-	-	-	-	-	-
92-092	19:50	2.188	19.1	*	*	-	2	*	1	-	1	-	-	-	-	-	-	-	-	-	-	-	-	-	-	-	-
92-107	18:05	2.155	14.9	*	*	-	-	*	-	-	-	-	-	-	-	-	-	-	-	-	-	-	-	-	-	-	-
92-114	21:59	2.137	7.2	*	*	-	-	*	2	-	-	-	-	-	-	-	-	-	-	-	-	-	-	-	-	-	-
92-135	12:59	2.078	20.6	*	*	-	-	*	-	-	-	-	-	-	-	-	-	-	-	-	-	-	-	-	-	-	-
92-155	18:50	2.010	20.2	*	*	-	-	*	1	-	-	-	-	-	-	-	-	-	-	-	-	-	-	-	-	-	-
92-177	19:14	1.923	22.0	*	*	-	-	*	1	-	-	-	-	-	-	-	-	-	-	-	-	-	-	-	-	-	-
92-192	18:18	1.857	15.0	*	*	-	-	*	-	-	1	-	-	-	-	-	-	-	-	-	-	-	-	-	-	-	-
92-215	20:04	1.744	23.1	*	*	-	-	*	-	-	1	-	-	-	-	-	-	-	-	-	-	-	-	-	-	-	-
92-239	23:10	1.612	24.1	*	*	-	1	*	-	-	-	-	-	-	-	-	-	-	-	-	-	-	-	-	-	-	-
92-261	22:39	1.480	22.0	*	*	-	-	*	-	-	-	-	-	-	-	-	-	-	-	-	-	-	-	-	-	-	-
92-315	00:48	1.140	53.1	*	*	-	1	*	-	-	1	-	-	-	-	-	-	-	-	-	-	-	-	-	-	-	-
92-329	01:01	1.058	14.0	*	*	-	-	*	-	-	-	-	-	-	-	-	-	-	-	-	-	-	-	-	-	-	-
92-343	15:10	0.984	14.6	*	*	-	-	*	1	-	-	-	-	-	-	-	-	-	-	-	-	-	-	-	-	-	-
92-353	00:00	0.984	9.4	*	*	-	-	*	1	-	-	-	-	-	-	-	-	-	-	-	-	-	-	-	-	-	-
92-363	16:09	1.007	10.7	*	*	-	2	*	1	-	1	-	-	-	-	-	-	-	-	-	-	-	-	-	-	-	-
Impacts (counted)				*	*	4	55	*	92	2	73	0	53	0	83	0	14	0	46	0	21	1	8	0	12	1	4
Impacts (complete data)				*	*	0	49	*	49	0	71	0	26	0	76	0	11	0	43	0	9	0	8	0	12	1	3
All events (complete data)				3225	958	33	49	86	88	17	71	5	29	1	76	0	11	0	43	0	9	0	8	0	12	1	3

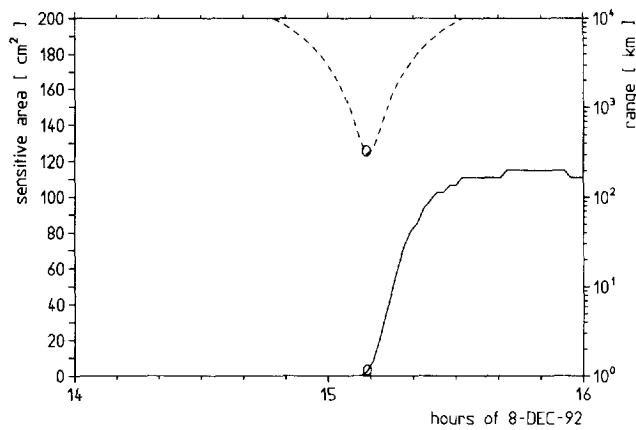


Fig. 5. Details of the second Earth flyby as a function of time. The distance from *Galileo* to Earth is given (dashed line) as is the area of the dust detector capable of detecting particles on circular prograde orbits about the Earth (solid line). A single dust particle was detected almost exactly at closest approach (open circles)

(R in AU), ecliptic longitude and latitude (LON, LAT) and the distance to the Earth (R_E in AU). This is followed by the rotation angle (ROT), as defined above. Whenever this value is indeterminate ($SEC = 0$), ROT is arbitrarily set to 999. This occurs 71 times. Ecliptic longitude and latitude (S_LON, S_LAT) of the positive sensor axis pointing are displayed next. (When ROT is not valid, then S_LON and S_LAT cannot be used.) Mean impact speed (\bar{v}) and speed error factor (VEF) as well as mean particle mass (m) and mass error factor (MEF) are presented last. We suggested that whenever $VEF > 6$, both speed and mass values should be discarded. This occurs for 21 impacts.

No intrinsic dust charge values are given because the noise rate was very high (Paper I). Furthermore, the signal amplitudes on the induced charge grid were similar for both noise and impact events. Therefore, reliable dust charge values are difficult to obtain and require careful study of the noise environment with the whole data set. This work is forthcoming.

During the second Earth flyby an impact of a “big” dust particle (No. 350) was recorded. This particle was detected at *Galileo*’s perigee 300 km above the Earth. It had a mass of 3×10^{-12} g and an impact speed of 33 km s^{-1} , which is compatible with a debris particle in a bound orbit about the Earth. No other debris particle was detected during this flyby. Figure 5 shows the sensitivity of the *Galileo* dust detector with respect to dust particles in prograde circular orbits around the Earth. Such particles are strongly concentrated at low altitudes and were nearly impossible to detect during the inbound trajectory of *Galileo*. No dust particles were detected during the previous flybys of Earth and Venus.

Analysis

In this section we will discuss various characteristics of the data set presented above. First we discuss the amplitude distribution of the impact charge. Then the in-flight channeltron amplification is determined. The derived mass and

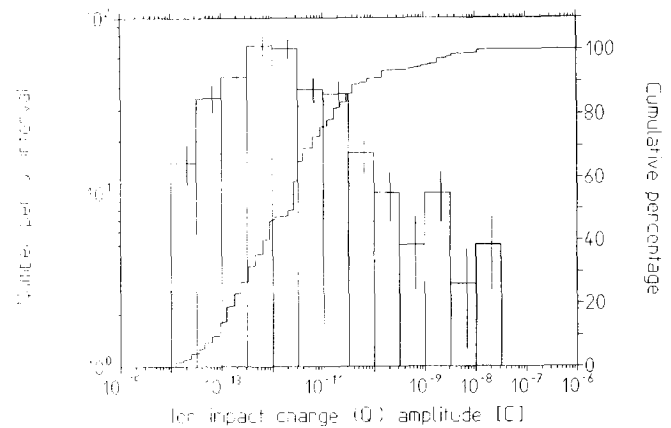


Fig. 6. Amplitude distribution of the impact charge Q_1 . Bars indicate numbers of impacts per charge interval, while the solid line shows the cumulative distribution. This curve is significantly flatter than a similar one for *Ulysses* (Paper III, Fig. 4), implying that *Galileo* is sensing larger particles

speed values are analyzed and finally the *Galileo* impact rates are compared with Divine’s (1993) meteoroid model.

Because of its relative insensitivity to noise, the positive impact charge Q_1 is the most important impact parameter determined by the *Galileo* dust detector. Figure 6 shows the distribution of the impact charge (Q_1) measured until the end of 1992. Impact charges are observed over the entire six orders of magnitude that the instrument is capable of measuring. About 2% of all impacts are close to the saturation limit and may constitute lower limits of the actual impact charges. Above about 10^{-12} C, the impact charge distribution closely follows a power law with index about $-1/3$ which is flatter than the $-1/2$ power law obeyed by *Ulysses* impacts (Paper III). This is a real effect which implies that, on average, *Galileo* is sensing larger particles than *Ulysses*. The number of impacts inducing charges below 10^{-12} C are reduced in Fig. 6; thus the low Q_1 impacts are not complete. The same is true when one looks at the charge distribution of *Ulysses* “big” impacts (Paper III, Fig. 4).

Both *Galileo* and *Ulysses* instruments showed high noise levels for the channeltron detector, even at low channeltron amplifications. To improve the noise behavior, we used a lower high voltage value (and hence amplification) than originally planned. In this paragraph, we determine the in-flight channeltron amplification. A measure of the amplification is the ratio of the channeltron charge Q_C over the ion charge Q_1 . This ratio is displayed in Fig. 7 as a function of the ion charge Q_1 at high voltage step $HV = 2$ (1020 V). The sensitivity threshold and the saturation limit of the channeltron charge are given as solid diagonal lines. The mean charge ratio Q_C/Q_1 (i.e. the channeltron amplification determined for $10^{-12} \text{ C} \leq Q_1 \leq 10^{-10} \text{ C}$) at this high voltage is $A \sim 1.6$.

Masses and speeds of all “big” impacts recorded until the end of 1992 are displayed in Fig. 8. Speeds have been found over the entire calibration range from 2 to 70 km s^{-1} and the masses vary over 10 orders of magnitude from 10^{-16} to 10^{-6} g. The mean errors are a factor 2 for the speed and a factor 10 for the mass. The clustering of the speed values are due to the discrete steps in the rise time

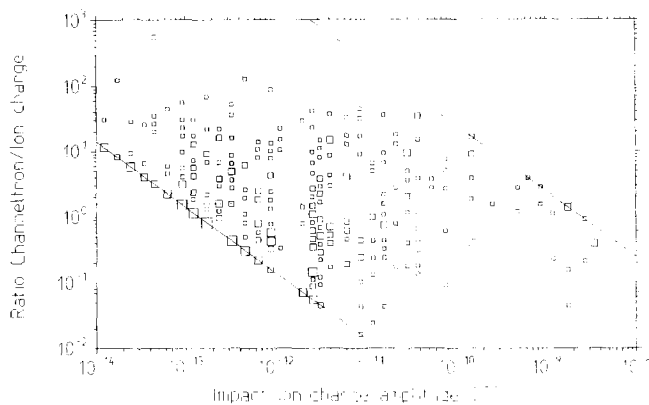


Fig. 7. Channeltron amplification factor $A = Q_C/Q_I$ as a function of impact charge Q_I for channeltron high voltage step 2 (1020 V). The area of the squares indicates the number of events included at each point

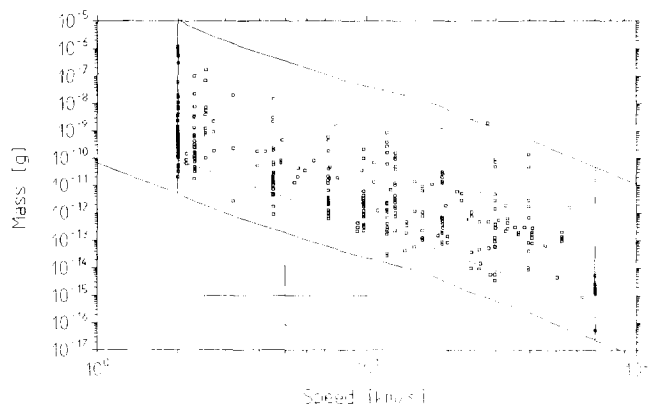


Fig. 8. Masses and impact speeds of all “big” impacts recorded by *Galileo*. The upper and lower solid lines indicate the threshold and saturation limits of the detector. The central dotted line is the effective mass threshold dividing “big” from “small” impacts for the *Ulysses* data. Applying the *Ulysses* result to the *Galileo* data set implies that the number of “big” impacts below this line should equal the number of “small” impacts above it (see Paper III)

measurement, but this quantization effect is much smaller than the uncertainty in the speed measurement. The large number of very low impact speeds (below 3 km s^{-1}) needs further study. The number of “big” impacts is incomplete in a band of width a factor one hundred in mass above the sensitivity threshold. Many of the “big” impacts (46%), however, occur in this band. Furthermore, the “small” impacts have yet to be recovered from the *Galileo* data. The effective mass thresholds for “big” impacts has been estimated for the more complete *Ulysses* data set (shown as the dotted line in Fig. 8). If we adopt the *Ulysses* results (cf. Paper III, Fig. 7), then the number of unseen “small” impacts above the dotted line should equal the number of detected “big” impacts below it. It should be remarked that this threshold for “big” impacts is rigorously valid only for the dust population (mass and speed distributions) recorded by the *Ulysses* dust detector. Therefore, by applying this threshold to the *Galileo* data it is assumed that the mass and speed distributions of the dust particles recorded by *Galileo* and *Ulysses* do not significantly differ. At masses $> 10^{-12} \text{ g}$, all “big” particles

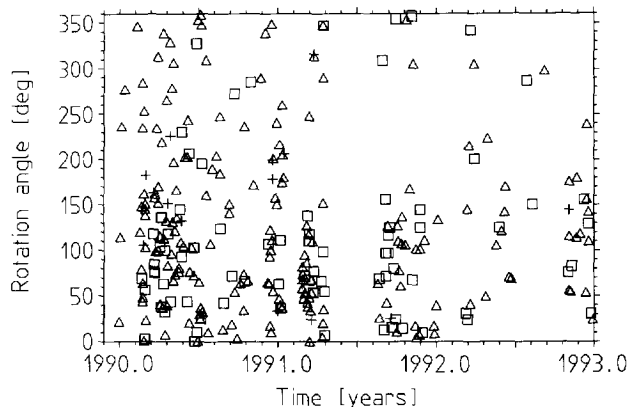


Fig. 9. Rotation angle vs time for two different mass ranges. Gaps in the data coverage show up as empty vertical bands. For some time periods no rotation angle information was available; these data are not shown. Symbols denote different mass–speed combinations. Squares and triangles are particles with masses $> 2.5 \times 10^{-14} \text{ g}$ while impacts denoted by plus signs are smaller. Squares are fast particles with speeds $> 15 \text{ km s}^{-1}$, whereas particles denoted by triangles are slower

except the slowest ($< 6 \text{ km s}^{-1}$) can be detected. Particles with smaller masses will not be completely recorded because those with slower speeds fall below the detection threshold.

Directions of the recorded “big” impacts are shown in Fig. 9: the rotation angles at the time of impact are shown as functions of time. Meteoroids moving parallel to the ecliptic plane should have rotation angles around 90° and 270° (see the discussion of the rotation angle above). Beside some gaps in the data, there are times when rotation angles are uniformly distributed and other times when they cluster in a limited rotation angle interval. Uniform distribution of rotation angles can occur when dust particles arrive at the spacecraft isotropically (at least in the spin plane), when dust particles arrive from close to the spin axis, and for other more complicated distributions. For most of the times, rotation angles cluster around 90° . This effect is most obvious during the second half of 1991 and the beginning of 1992. Modeling the impact directions as a consequence of the orbital distribution of interplanetary dust particles is in preparation.

Figure 4 shows the observed impact rate variations with time. During inbound (towards the Sun) portions of the interplanetary trajectory the dust detector pointed to the hemisphere opposite to the spacecraft motion; thus impact velocities were reduced and the observed impact rate is correspondingly low. In contrast, during the outbound portions of the *Galileo* trajectory the sensor points towards the hemisphere which includes the spacecraft ram direction and hence the observed impact flux is high. The general decrease of the dust flux with heliocentric distance is due to the decrease of the interplanetary dust population with increasing distance from the Sun. This flux variation is quantitatively modeled by Divine’s (1993) “Five populations of interplanetary meteoroids” model which is based on a variety of interplanetary dust observations including *Galileo* data from the first year (until the end of 1991). It is interesting to compare the impact rates observed by *Galileo* (Fig. 4) for the three-year period with

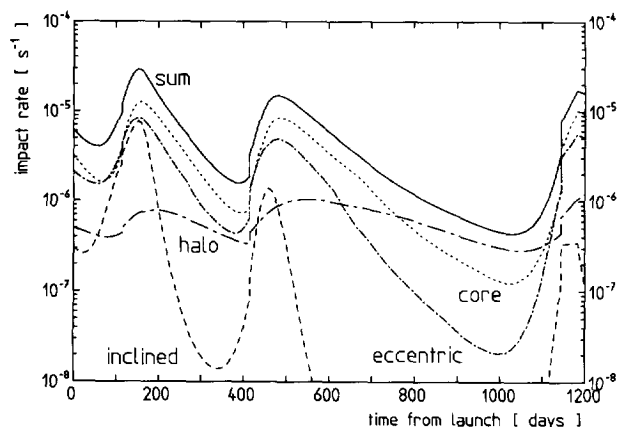


Fig. 10. Divine's (1993) model of the *Galileo* "big" impact rate (cf. Fig. 4). Contributions to the impact rate from five different dust populations are shown separately as well as summed together. The model calculations take into account the orbit of *Galileo* as well as the detector geometry and sensitivity

the model values (Fig. 10). The model values shown are adjusted for the new effective mass threshold for "big" impacts. This threshold is about a factor 10 below the value used by Divine in his original modeling. For most of the mission, the impact rates are matched by the core population which has been defined to represent the majority of interplanetary dust data including zodiacal light observations. At this stage, only impact rates are modeled by the Divine model. However, we are upgrading the model to include impact directions and impact speeds as well.

Besides comparing the dust observations with theoretical models, future data analysis activities will include identification of "small" impact events in the *Galileo* data set (cf. Baguhl et al., 1993), dead-time and measuring-time analysis of *Galileo* data, and finally, an analysis of measurements by the primary dust charge channel.

References

Baguhl, M., Grün, E., Linkert, D., Linkert, G. and Siddique, N., Performance of the Galileo and Ulysses dust detectors. *Proceeding of the Workshop on Hypervelocity Impacts in Space* (edited by J. A. M. McDonnell), pp. 153–159. University of Kent at Canterbury, 1992.

Baguhl, M., Grün, E., Linkert, D., Linkert, G. and Siddique, N.,

Identification of "small" dust impacts in the Ulysses dust detector data. *Planet. Space Sci.* **41**, 1085–1098, 1993.

Baguhl, M., Grün, E., Hamilton, D. P., Linkert, G., Riemann, R., Staubach, P. and Zook, H., The flux of interstellar dust observed by Ulysses and Galileo. *Space Sci. Rev.* **72**, 471–476, 1994.

D'Amario, L. A., Bright, L. E. and Wolf, A. A., Galileo trajectory design. *Space Sci. Rev.* **60**, 23–78, 1992.

Divine, N., Five populations of interplanetary meteoroids. *J. geophys. Res.* **98**, 17029–17048, 1993.

Grün, E., Zook, H. A., Fechtig, H. and Giese, R. H., Collisional balance of the meteoritic complex. *Icarus* **62**, 244–272, 1985.

Grün, E., Baguhl, M., Fechtig, H., Hanner, M. S., Kissel, J., Lindblad, B.-A., Linkert, D., Linkert, G., Mann, I., McDonnell, J. A. M., Morfill, G. E., Polansky, C., Riemann, R., Schwehm, G., Siddique, N. and Zook, H. A., Galileo and Ulysses dust measurements: from Venus to Jupiter. *Geophys. Res. Lett.* **19**, 1311–1314, 1992a.

Grün, E., Baguhl, M., Fechtig, H., Hanner, M. S., Kissel, J., Lindblad, B.-A., Linkert, D., Linkert, G., McDonnell, J. A. M., Morfill, G. E., Schwehm, G., Siddique, N. and Zook, A., Interplanetary dust near 1 AU. *Proceeding of the Workshop on Hypervelocity Impacts in Space* (edited by J. A. M. McDonnell), pp. 173–179. University of Kent at Canterbury, 1992b.

Grün, E., Fechtig, H., Giese, R. H., Kissel, J., Linkert, D., Maas, D., McDonnell, J. A. M., Morfill, G. E., Schwehm, G. and Zook, H. A., The Ulysses dust experiment. *Astron. Astrophys. Suppl. Ser.* **92**, 411–423, 1992c.

Grün, E., Fechtig, H., Hanner, M. S., Kissel, J., Lindblad, B.-A., Linkert, D., Linkert, G., Morfill, G. E. and Zook, H. A., The Galileo dust detector. *Space Sci. Rev.* **60**, 317–340, 1992d.

Grün, E., Hamilton, D. P., Baguhl, M., Riemann, R., Horanyi, M. and Polansky, C., Dust streams from comet Shoemaker–Levy 9? *Geophys. Res. Lett.* **21**, 1035–1038, 1994.

Grün, E., Baguhl, M., Divine, N., Fechtig, H., Hamilton, D. P., Hanner, M. S., Kissel, J., Lindblad, B.-A., Linkert, D., Linkert, G., Mann, I., McDonnell, J. A. M., Morfill, G. E., Polansky, C., Riemann, R., Schwehm, G., Siddique, N., Staubach, P. and Zook, H. A., Two years of Ulysses dust data. *Planet. Space Sci.* **43**, 971–999, 1995a.

Grün, E., Baguhl, M., Hamilton, D. P., Kissel, J., Linkert, D., Linkert, G. and Riemann, R., Reduction of Galileo and Ulysses dust data. *Planet. Space Sci.* **43**, 941–951, 1995b.

Hamilton, D. P. and Burns, J. A., Orbital stability zones about asteroids II. The destabilizing effects of eccentric orbits and of solar radiation. *Icarus* **96**, 43–64, 1992.

Johnson, T. V., Yeates, C. M. and Young, R., Space science reviews volume on Galileo mission overview. *Space Sci. Rev.* **60**, 3–21, 1992.

Riemann, R. and Grün, E., Meteor streams, asteroids and comets near the orbits of Galileo and Ulysses. *Proceeding of the Workshop on Hypervelocity Impacts in Space* (edited by J. A. M. McDonnell), pp. 120–125. University of Kent at Canterbury, 1992.